

Paper:

# Linear Quadratic Optimal Regulator for Steady State Drifting of Rear Wheel Drive Vehicle

Ronnapee Chaichaowarat and Witaya Wannasuphprasit<sup>†</sup>

Department of Mechanical Engineering, Chulalongkorn University  
254 Phayathai Road, Wangmai, Pathumwan, Bangkok 10330, Thailand  
E-mail: witaya.w@chula.ac.th

<sup>†</sup>Corresponding author

[Received April 15, 2014; accepted January 28, 2015]

**Drifting is a large sideslip cornering technique with counter steering, which is advantageous in some driving conditions where vehicle-handling capability over linear tire slip-friction characteristics is imperative. In this paper, the dynamics of a rear-wheel-drive (RWD) vehicle cornering at steady states was simplified using a single-track vehicle model. In addition, tire frictions in any slip conditions were estimated from the combination of the Pacejka's magic formula and the modified Nicolas-Comstock tire model. A computer program was developed, on the basis of the equations of motion (EOMs) derived via the body-fixed coordinate so that the suitable cornering speed and its corresponding steady-state driving control inputs (the steering angle and rear wheel slip ratio) could be calculated automatically for any given radius of curvature and vehicle sideslip. The other set of EOMs was derived via the normal-tangential coordinate and then linearized so that the state space description could be constructed. Eventually, the linear quadratic optimal regulator was designed and simulated via MATLAB for various regulation problems where the initial condition of each individual state deviated from its desired steady-state value. According to the simulation results, the physical explanation of the control inputs can be used as guidance for adjusting vehicle behavior in manual driving.**

**Keywords:** vehicle dynamics, automotive control, drifting, nonlinear control systems, quadratics optimal regulators

## 1. Introduction

Nowadays, a variety of active safety systems have been developed for general passenger vehicles so that drivers can control their vehicles even in emergency conditions [1]. Most of the existing systems – e.g., differential braking, active steering, and independent wheel torque control systems in modern electric or hybrid vehicles – are developed on the basis of a simplified vehicle model of steady-state cornering with small sideslip, as

in [2]. In addition, the elementary active safety systems in all current automobiles – an anti-lock braking system (ABS) and a traction control system (TCS) – are primarily intended to prevent extreme sliding so that all tires operate within the linear region of the tire slip-friction characteristic, allowing ordinary drivers to maintain control. It is envisioned that rather than restricting the tire slip limit within the linear region, both the full handling performance of vehicle and the expert skills of the driver in extreme slip conditions can be advantageous in terms of accident avoidance.

Drifting is a cornering technique with large sideslip as a result of the rear tires experiencing extreme slip in both the lateral and longitudinal directions. Although drifting is not convenient for a normal driver, in addition it requires expert skills to control the suitable slip of each of the tires to maintain the equilibrium of forces and the moment so that the vehicle travels along a desired trajectory. This technique is popular and is frequently used by expert rally drivers when turning sharply on dirt tracks to ensure that their vehicles are not understeered.

That the number of studies on drifting has increased significantly over the last decade reflects the increase in researcher awareness of how important an understanding of drifting is. According to the computational simulation in [3], though the minimum time trajectory cannot be acquired, drifting provides an advantage to return to a controllable straight-line driving state faster than small-slip driving. As a result, the driver has enough time to respond to emergencies or unexpected changes in the driving environment. Some basic drifting techniques – e.g., trail braking and pendulum turning – have been studied and simulated using experimental data recorded from drift testing by an expert rally driver in [4, 5]. The test vehicle had an inertial measurement unit, a GPS module, and other necessary equipment to measure the vehicle state. In addition, neural networks were used in [6] so that the vehicle sideslip could be simply related with the data measured from an accelerometer array. Although some controversy about the drifting dynamics had begun to be revealed by a number of works, very few studies have been conducted on the development of a controller for automatic drifting.

As previously mentioned, drifting with extreme slip may be advantageous in some cornering conditions. With



this vision in mind, steady-state drifting, which is the simplest case, was studied first. The optimal controller for steady-state drifting of an all-wheel-drive (AWD) vehicle was initiated in [7], where computational simulation was conducted via a single-track vehicle model along with the combination of the Bakker-Nyborg-Pacejka (BNP) magic formula [8] and the friction circle model, which assumes symmetrical tire characteristics in both the lateral and longitudinal directions. The linear quadratic optimal regulator (LQR) controller was designed corresponding to the state space model constructed from the linearization of the vehicle model and the tire model about the desired steady state. However, the steering angle was fixed so that the open-loop driving control inputs – the front- and rear-wheel slip ratios – could be directly computed without any iteration. As a result, it was difficult to generate most of the calculated control inputs in real-world situations. For example, independent torque distribution among the front and rear drive shafts was needed in case a positive slip ratio was required in both the front and rear wheels. In addition, the left-foot-braking technique may be required in case a negative slip ratio was required at the front wheels and a positive slip ratio was required at the rear wheels.

Hence, it would be more appropriate to derive control inputs that could be controlled conveniently. Without making the steering angle constant, the algorithms to calculate the control inputs for steady-state cornering of an RWD vehicle were developed in [9–13] by neglecting rolling resistance and assuming that no brake torque was applied to the front wheels. The optimal controller for steady-state drifting of an RWD vehicle was initiated and simulated computationally in [9, 10], where the comprehensive full-car vehicle model, along with the tire friction estimating approach as used in [7], was used to develop a computer program for iteration of the driving control inputs: the steering angle and the rear drive torque. However, details of the iteration algorithm were not provided. In addition, the tire friction estimation procedure used in [7, 9, 10] gave an estimation with discrepancies at a high degree of combined slip. Soon afterward, the computer program for automatic iteration of the steady-state control inputs – the steering angle and rear wheel slip ratio – was developed in [11] using the single-track vehicle model and the semi-empirical combined-slip Pacejka's magic formula tire model [14]. However, the tire model for simulation in [14] was too complicated for control purposes.

To estimate the tire frictions accurately despite extremely combined slip, the BNP-MNC tire friction model used in [12, 13] was developed from the combination of the BNP magic formula [8] and the modified Nicolas-Comstock (MNC) tire model [15, 16]. Building on the framework of [11], the computer program for calculation of a suitable cornering speed and its corresponding steady-state driving control inputs – the steering angle and rear wheel slip ratio – for any given radius of curvature and vehicle sideslip was developed in [12, 13] based on the single-track vehicle model and the BNP-MNC tire model.

Although the objective of finding control inputs for steady-state cornering in [12], as well in [11], was not for the control application but for the determination of the maximum cornering speed among different sideslips instead, those could be sufficiently fundamental for [12]. The feasible steady state – i.e., the cornering speed corresponding to a given radius of curvature and vehicle sideslip – acquired from the algorithm proposed in [12] were used as a reference for the desired steady state in [13] where the LQR stabilizing controller had been designed and simulated via MATLAB. In the proposed control scheme, stabilization is achieved by regulating the steering angle and rear slip ratio.

In this paper, the stabilizing controller developed in [13] is tested via computational simulation with a variety of regulation problems from which the initial condition of each individual state deviates from its desired steady-state value. The following content will be organized in the same way as in [13]. The single-track vehicle model will be introduced first. Then, the application of the BNP-MNC tire friction model will be briefly described. Afterward, the algorithm of computation for steady-state driving control inputs will be explained via the program flowchart. In addition, the equations of motion (EOMs) in terms of the state space description will be proposed for the control scheme. Next, the design procedure of the LQR stabilizing controller will be proposed. Finally, the simulation results will be presented and discussed from a physical perspective.

## 2. Vehicle Model

In this study, the dynamics of steady-state cornering of an RWD vehicle along a constant radius curve on a horizontal plane with a constant cornering speed and vehicle sideslip was simplified using a two-dimensional dynamic model – namely, the single-track model or the bicycle model. With the application of this model, the complexity of the actual automobile dynamics can be reduced with the consideration of a two-wheeled vehicle in which the dynamics of suspension and the effects of lateral load transfer are neglected.

### 2.1. Single Track Vehicle Model

To define the symbols used in the single-track vehicle model and their sign conventions, the translation of the vehicle drifting along the arc from position A to B is illustrated in **Fig. 1**.

In this figure, the  $x$ - $y$  coordinate is the moving frame affixed to the vehicle body at its center of gravity (CG), where the  $x$ -axis is oriented in the longitudinal direction directed toward the vehicle heading, and the  $y$ -axis is oriented in the lateral direction. The other moving frame located at the CG is the  $n$ - $t$  coordinate, the direction of which always changes depending on the direction of the vehicle velocity. Longitudinal distances  $L_f$  and  $L_r$  are measured from the CG to the front and rear axles, respec-

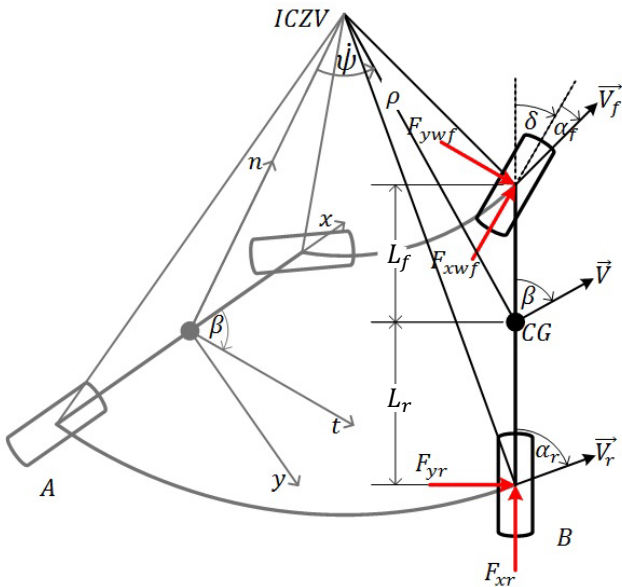


Fig. 1. Symbols used in the single-track vehicle model.

tively. The vehicle velocity  $\vec{V}$  measured at the CG is perpendicular to the direction of the curved radius  $\rho$ , which is measured from the instantaneous center zero velocity (ICZV). The angle between the actual velocity and the instant heading direction is given by the vehicle sideslip  $\beta$ . Likewise, the direction of local velocities measured at the front axle  $\vec{V}_f$  and rear axle  $\vec{V}_r$  are perpendicular to the directions of the curved radii measured from the ICZV to the front and rear axles, respectively. The sideslip  $\beta$ , the steering angle  $\delta$ , the front-wheel slip angle  $\alpha_f$ , and the rear-wheel slip angle  $\alpha_r$  are positive in the clockwise direction, whereas the yaw angle  $\psi$ , the yaw rate  $\dot{\psi}$ , and the yaw acceleration  $\ddot{\psi}$  are measured in the counterclockwise direction. Finally, the positive directions and the points of applications of all tire forces are indicated. In this paper, drifting is defined by the counter steering behavior – i.e., the positive steering angle ( $\delta > 0$ ) in the counterclockwise cornering.

According to the body-fixed  $x$ - $y$  coordinate, the set of equations of motion (EOMs) is obtained. The equilibriums of the forces in the longitudinal and lateral directions are shown in Eqs. (1) and (2), respectively. In addition, the equilibrium of the moment about the vertical axis is shown in Eq. (3).

$$F_{xwf} \cos \delta - F_{ywf} \sin \delta + F_{xr} = ma_x \quad (1)$$

$$F_{xwf} \sin \delta + F_{ywf} \cos \delta + F_{yr} = ma_y \quad (2)$$

$$-(F_{xwf} \sin \delta + F_{ywf} \cos \delta) L_f + F_{yr} L_r = I_{CG} \ddot{\psi} \quad (3)$$

The lateral and longitudinal accelerations can be derived from certain normal and tangential accelerations via the coordinate transformation between the  $x$ - $y$  and  $n$ - $t$  coordinates, as shown in Eqs. (4) and (5).

$$a_x = a_n \sin \beta + a_t \cos \beta \quad (4)$$

$$a_y = -a_n \cos \beta + a_t \sin \beta \quad (5)$$

In the special case of steady-state drifting, tangential acceleration is always zero, as expressed in Eq. (6). In addition, normal acceleration can be simply calculated from Eq. (7).

$$a_t = \rho \dot{\psi} + \rho \ddot{\psi} = 0 \quad (6)$$

$$a_n = \rho \dot{\psi}^2 = \frac{V_{ss}^2}{\rho_{ss}} \quad (7)$$

According to the assumptions that no rolling resistance and no braking and driving torques are applied to the front wheels, the EOMs describing steady-state drifting of an RWD vehicle can be modified as given in Eqs. (8)–(10).

$$-F_{ywf} \sin \delta + F_{xr} = \frac{mV_{ss}^2}{\rho_{ss}} \sin \beta_{ss} \quad (8)$$

$$F_{ywf} \cos \delta + F_{yr} = -\frac{mV_{ss}^2}{\rho_{ss}} \cos \beta_{ss} \quad (9)$$

$$-F_{ywf} \cos \delta L_f + F_{yr} L_r = 0 \quad (10)$$

The obtained EOMs were rearranged to a usable form as follows:

$$F_{ywf} = \frac{ma_y L_r}{(L_f + L_r) \cos \delta} \quad (11)$$

$$F_{xr} = ma_x + F_{ywf} \sin \delta \quad (12)$$

$$F_{yr} = ma_y - F_{ywf} \cos \delta \quad (13)$$

This set of EOMs was used to construct the computer program for calculation of the suitable cornering speed and corresponding open-loop driving control inputs for any desired steady state.

By using the single-track vehicle model, lateral load transfer can be neglected. However, longitudinal load transfer is still significant. The calculations of vertical loads at the front and rear axles are shown in Eqs. (14) and (15), respectively, where  $h$  is the vertical distance of the CG from the ground.

$$F_{zf} = \frac{m}{L_f + L_r} (gL_r - a_x h) \quad (14)$$

$$F_{zr} = \frac{m}{L_f + L_r} (gL_f + a_x h) \quad (15)$$

For a given set of vehicle states – the radius of curvature ( $\rho$ ), vehicle sideslip ( $\beta$ ), and cornering speed ( $V$ ), the vehicle yaw rate ( $\dot{\psi}$ ) can be computed directly, as shown in Eq. (16). In addition, the local velocities at the CG in each component are given in Eqs. (17) and (18).

$$\dot{\psi} = \frac{V}{\rho} \quad (16)$$

$$V_x = V \cos \beta \quad (17)$$

$$V_y = V \sin \beta \quad (18)$$

From the kinematic relation, the components of the front axle velocity along the longitudinal and lateral directions of the vehicle are given in Eqs. (19) and (20), respectively. In addition, the components parallel and perpendicular to

the wheel heading direction, which are required for the calculation of the slip angle and slip ratio, are given in Eqs. (21) and (22), respectively.

$$V_{xf} = V_x \dots \dots \dots (19)$$

$$V_{yf} = V_y - \dot{\psi}L_f \dots \dots \dots (20)$$

$$V_{xwf} = V_{xf} \cos \delta + V_{yf} \sin \delta \dots \dots \dots (21)$$

$$V_{ywf} = -V_{xf} \sin \delta + V_{yf} \cos \delta \dots \dots \dots (22)$$

Likewise, components parallel and perpendicular to the wheel heading direction of the rear axle velocity are given in Eqs. (23) and (24), respectively.

$$V_{xr} = V_x \dots \dots \dots (23)$$

$$V_{yr} = V_y + \dot{\psi}L_r \dots \dots \dots (24)$$

For the front tire radius of  $r_f$  and the rotational speed of  $\omega_f$ , the slip angle can be calculated by using Eq. (25) or (26), whereas Eq. (27) is for slip ratio calculation. For the rear tire radius of  $r_r$  and the rotational speed of  $\omega_r$ , the slip angle and slip ratio can be calculated by using Eqs. (28) and (29), respectively.

$$\alpha_f = \tan^{-1} \left( \frac{V_{ywf}}{V_{xwf}} \right) \dots \dots \dots (25)$$

$$\alpha_f = \tan^{-1} \left( \frac{V_{yf}}{V_{xf}} \right) - \delta \dots \dots \dots (26)$$

$$k_f = \frac{\omega_f r_f - V_{xwf}}{\omega_f r_f} \dots \dots \dots (27)$$

$$\alpha_r = \tan^{-1} \left( \frac{V_{yr}}{V_{xr}} \right) \dots \dots \dots (28)$$

$$k_r = \frac{\omega_r r_r - V_{xr}}{\omega_r r_r} \dots \dots \dots (29)$$

The slip angle and slip ratio obtained in this section are the important information directly affecting tire friction, as will be described in the following section.

**2.2. BNP-MNC Tire Friction Model**

While drifting, extremely combined slip at rear tires is inevitable. Thus, the appropriate tire friction model must be deliberately selected. In this study, the modified Nicolas-Comstock (MNC) tire model for combined slip [15] was used to estimate the tire frictions in both the longitudinal and lateral directions, as shown in Eqs. (30) and (31), respectively. The MNC tire model allows non-isotropic tire characteristics in both directions; ordinary tire slip-friction functions for pure slip in the longitudinal direction  $F_x(k)$  and the lateral direction  $F_y(\alpha)$  can be selected individually. The traction stiffness coefficient  $C_k$  and the cornering stiffness coefficient  $C_\alpha$  are given by the initial slope of  $F_x(k)$  and  $F_y(\alpha)$ , respectively. The first quotients of Eqs. (30) and (31) are the original Nicolas-Comstock model, as given in [16], and the second quotients are the correction factors that affect the shape of the friction ellipses.

**Table 1.** Magic formula parameters of a P225/60R16 tire.

Parameter	B	C	D	E	K	$F_z$ [N]
$F_x(k)$	0.12	1.48	3308	0.01	100	3101
$F_y(\alpha)$	0.08	1.44	6004	-1.84	100	6145

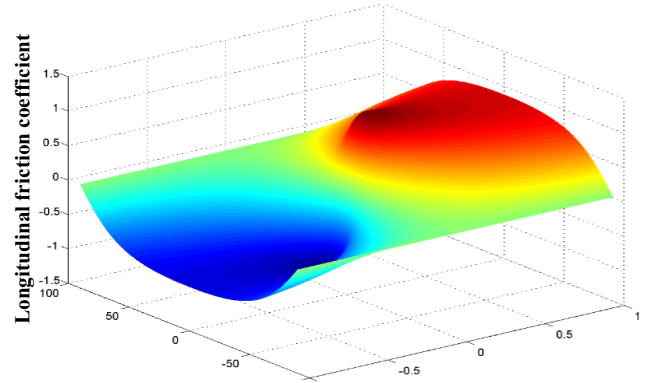


**Fig. 2.** Longitudinal friction coefficient versus slip.

$$F_x(\alpha, k) = \frac{F_x(k) F_y(\alpha) k}{\sqrt{k^2 F_y^2(\alpha) + F_x^2(k) \tan^2 \alpha}} \times \frac{\sqrt{k^2 C_\alpha^2 + (1 - |k|)^2 \cos^2 \alpha F_x^2(k)}}{k C_\alpha} \dots (30)$$

$$F_y(\alpha, k) = \frac{F_x(k) F_y(\alpha) \tan \alpha}{\sqrt{k^2 F_y^2(\alpha) + F_x^2(k) \tan^2 \alpha}} \times \frac{\sqrt{(1 - |k|)^2 \cos^2 \alpha F_y^2(\alpha) + \sin^2 \alpha C_k^2}}{C_k \sin \alpha} \dots (31)$$

In this study, the tire slip-friction functions for pure slip  $F_x(k)$  and  $F_y(\alpha)$  were formulated in terms of the Bakker-Nyborg-Pacejka (BNP) magic formula [8] as given in Eqs. (32) and (33).

$$F_i(s_i) = D_i \sin [C_i \tan^{-1} (B_i \theta_i)] \dots \dots \dots (32)$$

$$\theta_i = (1 - E_i) K_i s_i + \left( \frac{E_i}{B_i} \right) \tan^{-1} (B_i K_i s_i) \dots \dots (33)$$

where the subscript  $i = xy$  indicates the direction of interest, whether it is the longitudinal or the lateral direction of the friction and the slip. The longitudinal slip ( $s_x$ ) refers to the slip ratio ( $k$ ), whereas the lateral slip ( $s_y$ ) refers to the slip angle ( $\alpha$ ). The other symbols are the magic formula parameters.

By using the BNP-MNC tire friction model with the magic formula parameters gathered from the experiment of a P225/60R16 tire in [14], as shown in **Table 1**, the estimation results of the longitudinal tire friction coefficient ( $\mu_x = F_x/F_z$ ) can be plotted with varied slip angles and slip ratios as shown in **Fig. 2**. In a similar manner, the estimation results of the lateral tire friction coefficient

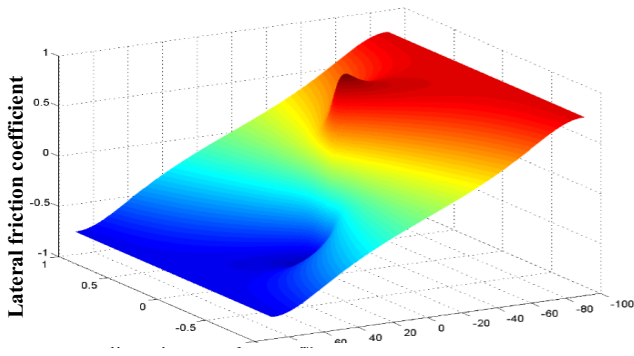


Fig. 3. Lateral friction coefficient versus slip.

( $\mu_y = F_y/F_z$ ) are plotted with varied slip angles and slip ratios as shown in Fig. 3.

According to Fig. 2, at any given slip ratio, maximum magnitude of longitudinal friction occurs at the zero slip angle when the tire does not slip in the lateral direction. At the zero slip angle, the longitudinal friction increases linearly with the increasing slip ratio and then reaches the maximum value. Finally, it slightly decreases to saturation until the slip ratio reaches unity. According to Fig. 3, at any given slip angle, maximum magnitude of lateral friction occurs at the zero slip ratio when the tire does not slip in the longitudinal direction. At the zero slip ratio, the lateral friction increases linearly with the increasing slip angle and then reaches the maximum value. Finally, it slightly decreases to saturation until the slip angle reaches  $90^\circ$ .

### 3. Computation of Feasible Steady-State Drifting and Control Inputs

As previously mentioned, without making the steering angle constant, computational iteration is necessary for the derivation of steady-state control inputs for RWD vehicle drifting. The vehicle model and the tire friction model described in the previous section were used to construct the computer program for the calculation of a suitable cornering speed for a given radius of curvature and vehicle sideslip. In addition, the corresponding driving control inputs for the steering angle and the rear-wheel slip ratio were calculated. The algorithm of the developed computation will be briefly described via the program flowchart in Fig. 4.

First, the vehicle parameters of vehicle mass ( $m$ ); moment of inertia ( $I_{CG}$ ); wheelbase ( $L$ ); longitudinal distance from the CG to the front axle ( $L_f$ ) and to the rear axle ( $L_r$ ); vertical distance of the CG from the ground ( $h$ ); and the BNP magic formula parameters ( $B, C, D, E,$  and  $K$ ) were defined. Then, the radius of curvature ( $\rho$ ), vehicle sideslip ( $\beta$ ), and positive initial estimation of the cornering speed ( $V$ ) had to be entered into the program. After that, the components of the acceleration in the  $n-t$  and  $x-y$  directions were computed by

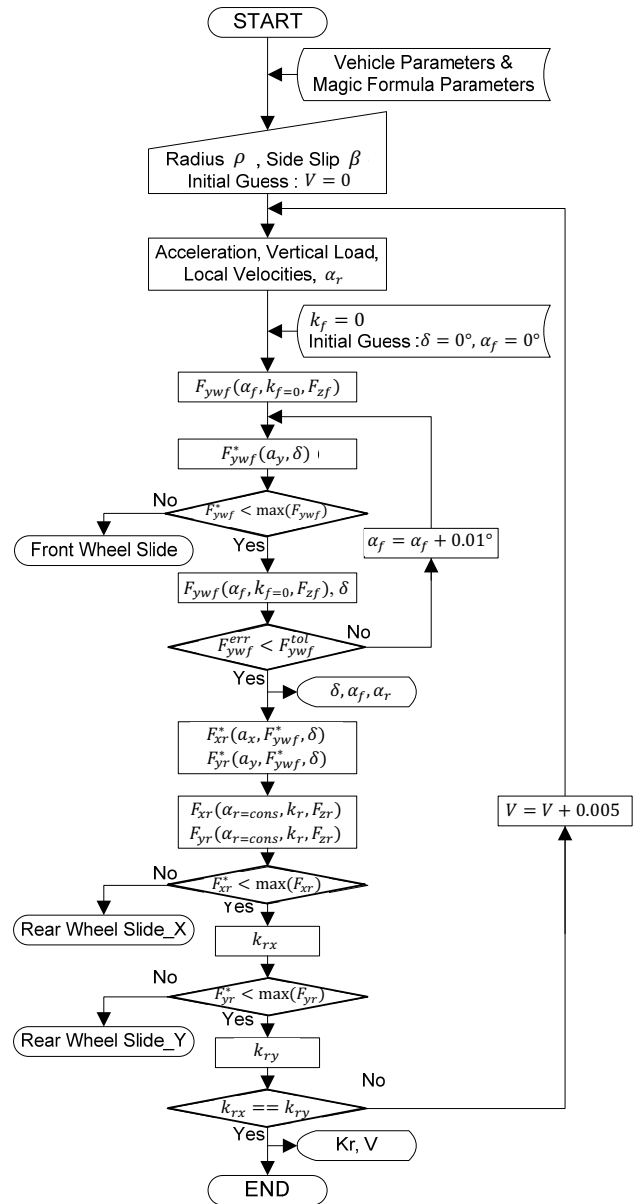


Fig. 4. Algorithm to compute steady-state control inputs.

Eqs. (4)–(7). The vertical loads at the front and rear axles were also computed using Eqs. (14) and (15). In addition, the vehicle yaw rate and local velocities at the CG, also at the front and rear axles, were calculated using Eqs. (16)–(24). Finally, the rear slip angle was directly calculated by Eq. (28).

For the ensuing iteration, the initial value of the steering angle must be set as any arbitrary constant – e.g., zero degrees ( $\delta = 0^\circ$ ) – so that the first iteration of the front lateral tire force  $F_{yw}^*(a_y, \delta)$  based on the modified vehicle model in Eq. (11) can be computed. In addition, the front slip angle, which will be increased by  $0.01^\circ$  at every loop of iteration, was primarily set at zero degrees ( $\alpha_f = 0^\circ$ ). The front tire lateral friction, varying with the slip angle at the zero slip ratio  $F_{yw}(\alpha_f, k_f=0, F_{zf})$ , was estimated by the BNP-MNC tire model. The lateral force

**Table 2.** Vehicle parameters used in the simulation.

Parameters	Value	Parameters	Value
$m$ [kg]	1250	$L$ [m]	2.52
$I_{CG}$ [kg·m <sup>2</sup> ]	2500	$h$ [m]	0.28
$L_f$ [m]	1.13	$r_f$ [m]	0.3
$L_r$ [m]	1.39	$r_r$ [m]	0.3

computed from the vehicle model ( $F_{ywf}^*$ ) was compared with the maximum of lateral friction estimated by the tire model ( $F_{ywf}$ ) to identify whether the front tire was still in equilibrium. The front tire will slide out in the lateral direction if the vehicle model-based tire force exceeds the maximum limit of friction generated from the tire model. If the front tire can sustain equilibrium, the corresponding front slip angle will be gained by iteration when the error deviation between the vehicle model-based tire force and the tire model-based tire force ( $F_{ywf}^{err}$ ) is less than the tolerance limit ( $F_{ywf}^{tol}$ ). In addition, the steering angle can be directly computed by Eq. (26).

The obtained steering angle was used to compute the rear-axle longitudinal force  $F_{xr}^*(a_x, F_{ywf}^*, \delta)$  and lateral force  $F_{yr}^*(a_y, F_{ywf}^*, \delta)$  using the modified vehicle model in Eqs. (12) and (13), respectively. In addition, both the longitudinal friction  $F_{xr}(\alpha_{r=cons}, k_r, F_{zr})$  and lateral friction  $F_{yr}(\alpha_{r=cons}, k_r, F_{zr})$  of the rear tire, varying with the slip ratio ( $k_r$ ) from 0 to 1, were estimated by using the BNP-MNC tire model at a previously calculated constant rear slip angle.

The vehicle model-based tire forces ( $F_{xr}^*, F_{yr}^*$ ) in both the longitudinal and lateral directions were separately compared with the tire model-based frictions ( $F_{xr}, F_{yr}$ ) to identify whether the rear tire was still in equilibrium. The rear tire will slide out in some direction if the vehicle model-based tire force exceeds the maximum limit of the friction generated from the tire model in that direction. If the rear tire could sustain equilibrium in both directions, the longitudinal friction-based rear tire slip ratio ( $k_{rx}$ ), which entails equality between the tire model-based friction ( $F_{xr}$ ) and vehicle model-based tire force ( $F_{xr}^*$ ), was specified. Likewise, the lateral friction-based rear tire slip ratio ( $k_{ry}$ ), which entails equality among the tire model-based friction ( $F_{yr}$ ) and vehicle model-based tire force ( $F_{yr}^*$ ), was specified simultaneously. The existence of the tangible slip ratio was at a suitable cornering speed when both rear slip ratios were equivalent ( $k_{rx} = k_{ry}$ ).

In this study, the vehicle parameters in **Table 2** were used for simulation. The results of the demo computation using the developed program are shown in **Fig. 5**. The attentive radius of curvature, the vehicle sideslip, and the arbitrary positive initial estimation of the cornering speed must be entered at the beginning. Then, the magnitude of the suitable steady-state velocity and the corresponding driving control inputs – the steering angle and rear wheel slip ratio, along with other important data, such as front- and rear-wheel slip angles and the tangible wheel rota-

Radius of Curvature (m)	22
Side Slip (deg)	15
Initial Guess of Velocity (km/h)	10
For Steady State Velocity	50.175 km/h
Steering Angle is	4.401 deg
Front Wheel Slip Angle is	7.720 deg
Rear Wheel Slip Angle is	18.436 deg
The Suitable Slip Ratio is	0.171
Error of Fxr is	1.989 Percent
Angular Speed of Front Wheel is	434.327 rpm
Angular Speed of Rear Wheel is	516.921 rpm
⋮	
For Steady State Velocity	50.230 km/h
Steering Angle is	4.326 deg
Front Wheel Slip Angle is	7.795 deg
Rear Wheel Slip Angle is	18.436 deg
The Suitable Slip Ratio is	0.169
Error of Fxr is	0.457 Percent
Angular Speed of Front Wheel is	434.726 rpm
Angular Speed of Rear Wheel is	516.242 rpm

**Fig. 5.** Demo results of the developed program.

tional speeds at the front and rear axles – were computed and displayed, respectively. From the given set of the entered data, only the simulation results corresponding to the feasible minimum and maximum cornering speeds are exhibited, respectively, in **Fig. 5**. In this paper, drifting is defined by the positive steering angle, which indicates counter-steering behavior.

## 4. Design of Stabilizing Controller for Steady-State Drifting

### 4.1. State Space Description

To design the linear quadratic optimal regulator (LQR) stabilizing controller, the new set of EOMs must be derived into the expression of the vehicle states and driving control inputs and then linearized into the state space description.

The equilibrium equations corresponding to the direction of absolute velocity at the CG were taken into consideration; therefore, they could then be derived in terms of tangential acceleration ( $a_t$ ), normal acceleration ( $a_n$ ), and yaw acceleration ( $\ddot{\psi}$ ) as Eqs. (34)–(36), respectively.

$$\frac{d}{dt}V = \frac{1}{m} [F_{xwf} \cos(\delta - \beta) - F_{ywf} \sin(\delta - \beta) + F_{xr} \cos \beta + F_{yr} \sin \beta] \dots \dots (34)$$

$$\frac{d}{dt}\beta = \frac{1}{mV} [F_{xwf} \sin(\delta - \beta) + F_{ywf} \cos(\delta - \beta) - F_{xr} \sin \beta + F_{yr} \cos \beta + mV\dot{\psi}] \dots (35)$$

$$\frac{d}{dt}\dot{\psi} = \frac{1}{I_{CG}} [- (F_{xwf} \sin \delta + F_{ywf} \cos \delta) a + F_{yr} b] (36)$$

According to the kinematic relation Eq. (37), the EOMs of an RWD vehicle drifting on a plane could be expressed by the implicit functions of the state variables and the driving control inputs as Eqs. (38)–(40) by neglecting rolling

resistance and assuming that no brake torque was applied to the front wheel.

$$\frac{d}{dt}\rho = \frac{\left(\dot{\psi} \frac{d}{dt}V - V \frac{d}{dt}\dot{\psi}\right)}{\dot{\psi}^2} \dots \dots \dots (37)$$

$$\begin{aligned} \frac{d}{dt}\rho &= f_1(\rho, \beta, V, \delta, k_r) \\ &= \frac{\rho}{mV} [-F_{ywf} \sin(\delta - \beta) + F_{xr} \cos \beta + F_{yr} \sin \beta] \\ &\quad + \frac{\rho^2}{I_{CG}V} [F_{ywf} \cos \delta a - F_{yr} b] \dots \dots \dots (38) \end{aligned}$$

$$\begin{aligned} \frac{d}{dt}\beta &= f_2(\rho, \beta, V, \delta, k_r) \\ &= \frac{1}{mV} \left[ F_{ywf} \cos(\delta - \beta) - F_{xr} \sin \beta \right. \\ &\quad \left. + F_{yr} \cos \beta + m \frac{V^2}{\rho} \right] \dots \dots \dots (39) \end{aligned}$$

$$\begin{aligned} \frac{d}{dt}V &= f_3(\rho, \beta, V, \delta, k_r) \\ &= \frac{1}{m} [-F_{ywf} \sin(\delta - \beta) + F_{xr} \cos \beta \\ &\quad + F_{yr} \sin \beta] \dots \dots \dots (40) \end{aligned}$$

The standard form of the state space description as Eqs. (41) and (42) could then be established by linearization of Eqs. (38)–(40) about the desired equilibrium  $(\rho_{ss}, \beta_{ss}, V_{ss})$ .

$$\dot{\tilde{\mathbf{X}}} = \mathbf{A}_{ss}\tilde{\mathbf{X}} + \mathbf{B}_{ss}\tilde{\mathbf{U}} \dots \dots \dots (41)$$

$$\tilde{\mathbf{Y}} = \mathbf{C}\tilde{\mathbf{X}} \dots \dots \dots (42)$$

The Jacobian matrices  $\mathbf{A}_{ss}$  and  $\mathbf{B}_{ss}$  were constructed by performing the partial derivative of Eqs. (38)–(40) by each of the state variables and each of the driving control inputs about the desired equilibrium, as given in Eqs. (43) and (44), respectively. Furthermore, the output matrix  $\mathbf{C}$  was the identity matrix with a dimension of  $3 \times 3$ .

$$\mathbf{A}_{ss} = \begin{bmatrix} \left. \frac{\partial f_1}{\partial \rho} \right|_{ss} & \left. \frac{\partial f_1}{\partial \beta} \right|_{ss} & \left. \frac{\partial f_1}{\partial V} \right|_{ss} \\ \left. \frac{\partial f_2}{\partial \rho} \right|_{ss} & \left. \frac{\partial f_2}{\partial \beta} \right|_{ss} & \left. \frac{\partial f_2}{\partial V} \right|_{ss} \\ \left. \frac{\partial f_3}{\partial \rho} \right|_{ss} & \left. \frac{\partial f_3}{\partial \beta} \right|_{ss} & \left. \frac{\partial f_3}{\partial V} \right|_{ss} \end{bmatrix} \dots \dots \dots (43)$$

$$\mathbf{B}_{ss} = \begin{bmatrix} \left. \frac{\partial f_1}{\partial \delta} \right|_{ss} & \left. \frac{\partial f_1}{\partial k_r} \right|_{ss} \\ \left. \frac{\partial f_2}{\partial \delta} \right|_{ss} & \left. \frac{\partial f_2}{\partial k_r} \right|_{ss} \\ \left. \frac{\partial f_3}{\partial \delta} \right|_{ss} & \left. \frac{\partial f_3}{\partial k_r} \right|_{ss} \end{bmatrix} \dots \dots \dots (44)$$

The state vector  $\tilde{\mathbf{X}}$  represented the deviation of the current states from the desired states, as given in Eq. (45).

In addition, the input vector  $\tilde{\mathbf{U}}$  represented the deviation of the current control inputs from the steady-state control inputs, as shown in Eq. (46).

$$\tilde{\mathbf{X}} = \begin{bmatrix} \rho - \rho_{ss} \\ \beta - \beta_{ss} \\ V - V_{ss} \end{bmatrix} \dots \dots \dots (45)$$

$$\tilde{\mathbf{U}} = \begin{bmatrix} \delta - \delta_{ss} \\ k_r - k_{r,ss} \end{bmatrix} \dots \dots \dots (46)$$

**4.2. LQR Stabilizing Controller**

In this study, the state variable feedback controller gain for steady-state drifting stabilization was designed to minimize the quadratic performance index in Eq. (47).

$$J = \frac{1}{2} \int_{t_0}^T (\tilde{\mathbf{X}}^T \mathbf{Q} \tilde{\mathbf{X}} + \tilde{\mathbf{U}}^T \mathbf{R} \tilde{\mathbf{U}}) dt \dots \dots \dots (47)$$

Appropriate choices for the composition of the weighting matrices – i.e., the semi-positive definite matrix  $(\mathbf{Q} \geq \mathbf{0})$  and the positive definite matrix  $(\mathbf{R} > \mathbf{0})$  – were suggested as Eqs. (48) and (49), respectively.

$$\frac{1}{Q_{ii}} = (t_f - t_0) \times \text{Max acceptable value of } [x_i(t)]^2 \quad (48)$$

$$\frac{1}{R_{ii}} = (t_f - t_0) \times \text{Max acceptable value of } [u_i(t)]^2 \quad (49)$$

The subscript  $i$  of the elements in the weighing matrices indicates the considered state or the control input. For example,  $Q_{11}$  is used for the gain consideration of the first state variable. The final time ( $t_f$ ) is determined by the desired setting time for state regulation. Deviation of the considered state varying with time from the desired steady state is denoted by  $(x_i(t))$ . Likewise, deviation of the considered control input varying with time from the steady state reference is denoted by  $(u_i(t))$ .

**5. Simulation Results**

The designed LQR stabilizing controller was simulated via MATLAB for various regulation problems, in which the initial condition of each individual state deviated from its desired steady state – the 22 m radius of curvature ( $\rho_{ss}$ ), 15° sideslip ( $\beta_{ss}$ ), and 50.23 km/h cornering speed ( $V_{ss}$ ). In this section, the simulation results for the regulation of the initial error in the radius of curvature, the initial error in the vehicle sideslip and the initial error in the cornering speed will be discussed from a physical perspective. The resulting plots of each case will exhibit the error of the radius of curvature, the error of the vehicle sideslip, the error of the cornering speed, the steering angle control input, and the rear-wheel slip ratio control input, changing with time, respectively.

**5.1. Regulation of Initial Error in Curve Radius**

The simulation results of the steady-state drifting stabilization when the initial radius of curvature deviated 1 m

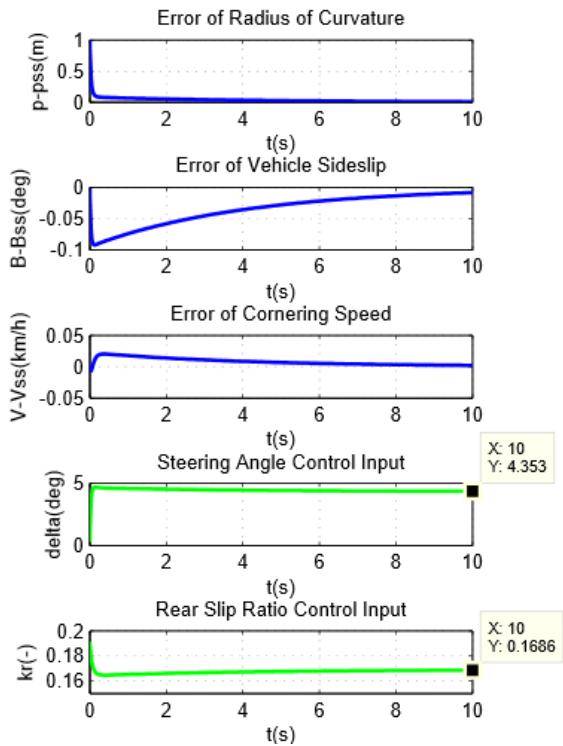


**Fig. 6.** Resulting plots for regulation of initial error in radius of curvature.

from its desired steady state ( $\rho_0 = 23$  m) are shown in **Fig. 6**. According to the plots of state errors, the error of the radius suddenly decreases to zero, resulting in an increase in the sideslip and speed error. However, all state errors were eventually eliminated by stabilization.

Based on the plots of the control inputs, a sharp drop in the steering angle below its steady reference ( $\delta_{ss} = 4.326^\circ$ ) was observed at the beginning of the simulation. This implies that the steering angle tends to be conventional steering such that the radius of curvature is reduced and then increases to its steady reference with a small overshoot. The plots of the state errors depicts that the sharp drop in the steering angle at the beginning affected the decrease of the sideslip and, later, the increase of the speed. In addition, the sharp rise of the rear slip ratio above its steady reference ( $k_{ss} = 0.169$ ) at the beginning of simulation affects the reduction of the lateral friction at the rear tire so that the decrease of the vehicle sideslip slowed down and returned to its desired value.

Furthermore, the trajectory plot of the RWD vehicle drifting on the  $X$ - $Y$  plane is shown in **Fig. 7**. The plot depicts that the controlled vehicle could drift at a steady state with a constant radius of curvature, sideslip, and cornering speed.

**5.2. Regulation of Initial Error in Vehicle Sideslip**

The simulation results of the steady-state drifting stabilization when the initial sideslip of the vehicle deviated  $2^\circ$  from its desired steady state ( $\beta_0 = 17^\circ$ ) is shown in **Fig. 8**. According to the plots of the state errors, the error of the

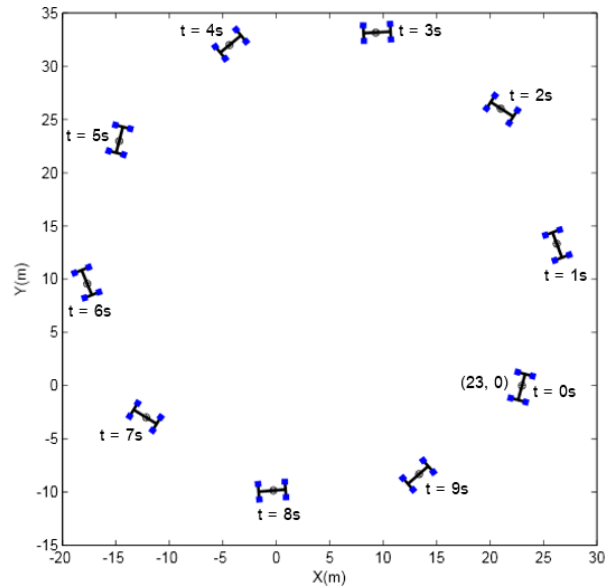


**Fig. 7.** Trajectory of the RWD vehicle drifting on the  $X$ - $Y$  plane.

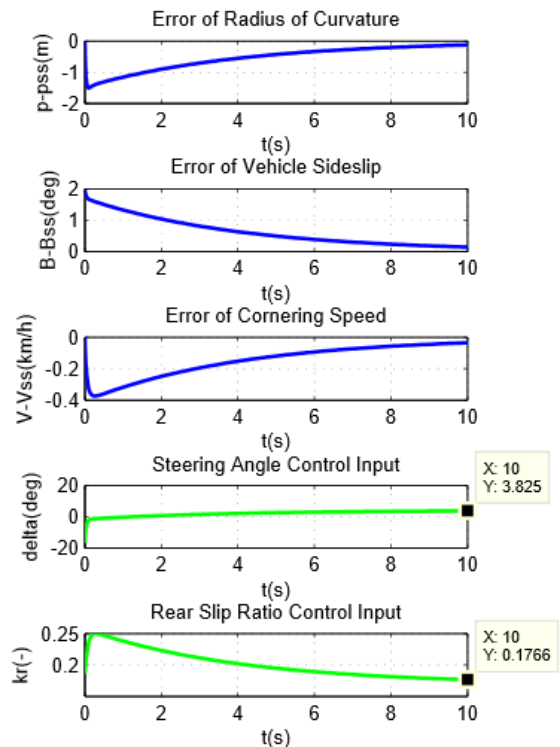


**Fig. 8.** Resulting plots for regulation of initial error in vehicle sideslip.

sideslip slowly decreased to zero, resulting in a sudden increase of the radius and speed error. However, all state errors were eventually eliminated by stabilization.

Based on the plots of control inputs, an extremely sharp drop in the steering angle below its steady-state value at the beginning of simulation could be observed. This implies that the steering angle was regulated to be hard conventional steering to reduce the exceeding sideslip. This

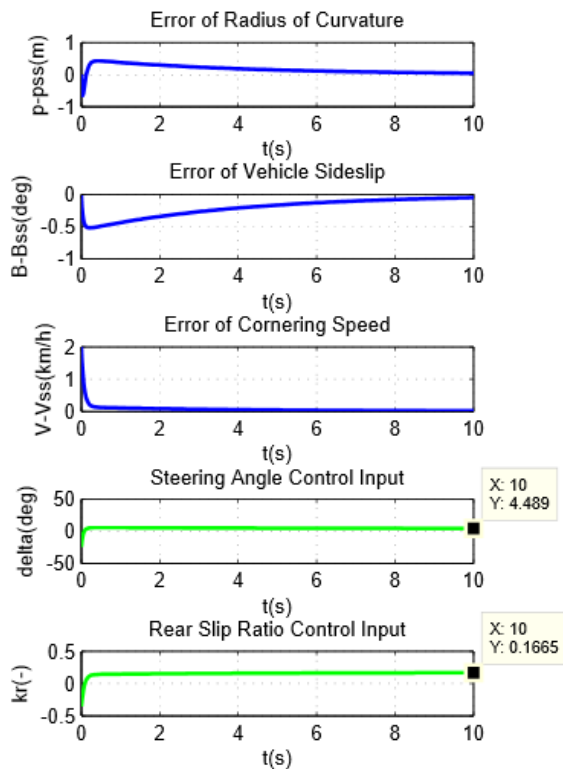


Fig. 9. Resulting plots for regulation of initial error in cornering speed.

response of the steering angle also directly affects the decrease of the radius of curvature. The steering angle increased to a positive value and eventually reached its steady reference. At the beginning of the simulation, the rear slip ratio increased sharply to cancel the effect of the sharply increased steering angle. At the same time that the steering angle became positive, the rear slip ratio decreased to its steady reference so that the rear tire could generate greater lateral friction to reduce the sideslip error.

### 5.3. Regulation of Initial Error in Cornering Speed

The simulation results of the steady-state drifting stabilization when the initial cornering speed deviated 2 km/h from its desired steady state ( $V_0 = 52.23$  km/h) are shown in Fig. 9. According to the plots of the state errors, the error of speed suddenly decreased to zero, resulting in an increase of the radius and sideslip error. However, all state errors were eventually eliminated by stabilization.

Based on the plots of the control inputs, a negative rear slip ratio at the beginning of the simulation to reduce the instant speed could be observed. This response of the rear slip ratio also directly affects the sudden decrease of the sideslip. Furthermore, the steering angle was regulated to be hard conventional steering at the beginning of the simulation to prevent too much negative deviation of the vehicle sideslip. This response of the steering angle also directly affects the negative deviation of the radius of curvature.

## 6. Conclusions

In this study, the single-track vehicle model and the BNP-MNC tire friction model were used to simplify the dynamics of RWD vehicle cornering at a steady state. The computer program for the calculation of a suitable cornering speed and its corresponding steady-state control inputs for any given radius of curvature and vehicle sideslip was developed on the basis of the EOMs derived via the body-fixed coordinate. The LQR stabilizing controller was designed from the state space description linearized from the other set of EOMs derived via the  $n-t$  coordinate; in addition, it was simulated by MATLAB, and the initial condition of each individual state deviated from its desired steady-state value. According to the simulation results, all state errors could be regulated. The discussion on the response of the control inputs may be used as guidance for adjusting vehicle behavior in manual driving. The steady-state drifting controller can be improved from other nonlinear system control schemes [17]. The application of an automatic drifting assistant system in general passenger vehicles may be feasible in the future.

### Acknowledgements

This research was partly funded by the Junior Science Talent Project (JSTP) and the Department of Mechanical Engineering at Chulalongkorn University.

### References:

- [1] N. Wada, A. Takahashi, M. Saeki, and M. Nishimura, "Vehicle yaw control using an active front steering system with measurements of lateral tire force," *J. of Robotics and Mechatronics*, Vol.23, No.1, pp. 83-93, 2011.
- [2] T. D. Gillespie, "Fundamentals of Vehicle Dynamics," SAE Int., PA, USA, 1992.
- [3] E. Velenis and P. Tsiotras, "Minimum time vs maximum exit velocity path optimization during cornering," *the IEEE Int. Symposium on Industrial Electronics*, 2005.
- [4] E. Velenis, P. Tsiotras, and J. Lu, "Modeling aggressive maneuvers on loose surfaces: data analysis and input parameterization," *the Mediterranean Conf. on Control and Automation*, 2007.
- [5] E. Velenis, P. Tsiotras, and J. Lu, "Modeling aggressive maneuvers on loose surfaces: the cases of trail-braking and pendulum-turn," *the European Control Conf.*, 2007.
- [6] M. Abdulrahim, "On the dynamics of automobile drifting," SAE Technical Paper, No.2006-01-1019, 2006.
- [7] E. Velenis, E. Frazzoli, and P. Tsiotras, "On steady-state cornering equilibria for wheeled vehicles with drift," *the 48th IEEE Conf. on Decision and Control*, pp. 3545-3550, 2009.
- [8] E. Bakker, L. Nyborg, and H. B. Pacejka, "Tyre modeling for use in vehicle dynamics studies," SAE Technical Paper, No.870421, 1987.
- [9] E. Velenis, D. Katzourakis, E. Frazzoli, P. Tsiotras, and R. Happee, "Stabilization of steady-state drifting for a RWD vehicle," *the 10th Int. Symposium on Advanced Vehicle Control*, 2010.
- [10] E. Velenis, D. Katzourakis, E. Frazzoli, P. Tsiotras, and R. Happee, "Steady-state drifting stabilization of RWD vehicles," *Control Engineering Practice*, Vol.10, No.11, pp. 1363-1376, 2011.
- [11] R. Chaichaowarat and W. Wannasuphprasit, "Two dimensional dynamic model of drifting vehicle," *the 7th TSAE Int. Conf. on Automotive Engineering*, 2011.
- [12] R. Chaichaowarat and W. Wannasuphprasit, "Dynamics and simulation of RWD vehicle drifting at steady state using BNP-MNC tire model," SAE Technical Paper, No.2013-01-0001, 2013.
- [13] R. Chaichaowarat and W. Wannasuphprasit, "Optimal control for steady state drifting of RWD vehicle," *Proc. of the 7th IFAC Symposium of Advances in Automotive Control*, pp. 824-830, 2013.

- [14] H. T. Szostak, W. R. Allen, and T. J. Rosenthal, "Analytical modeling of driver response in crash avoidance maneuvering. volume II: an interactive model for driver/vehicle simulation," U.S. Department of Transportation Report, NHTSA DOT HS-807-271, 1988.
- [15] R. Branch and M. Branch, "The tire-force ellipse (friction ellipse) and tire characteristics," SAE Technical Paper, No.2011-01-0094, 2011.
- [16] V. T. Nicolas and T. R. Comstock, "Predicting directional behavior of tractor semitrailers when wheel anti-skid brake systems are used," ASME Paper, No.72 - WA/AUT-16, 1972.
- [17] M. Tanaka, H. Ohtake, and K. Tanaka, "A simple, natural and effective framework of nonlinear systems control and its application to aerial robot," J. of Robotics and Mechatronics, Vol.26, No.2, pp. 140-147, 2014.



**Name:**  
Ronnapree Chaichaowarat

**Affiliation:**  
Department of Mechanical Engineering, Chulalongkorn University

**Address:**

254 Phayathai Road, Wangmai, Pathumwan, Bangkok 10330, Thailand

**Brief Biographical History:**

2012 Received Bachelor degree in Mechanical Engineering from Chulalongkorn University (1st Class Honors)

2013 Received Master degree in Mechanical Engineering from Chulalongkorn University

2013- Ph.D. Student, Department of Mechanical Engineering, Chulalongkorn University

**Main Works:**

- "Tire Test for Drifting Dynamics of a Scaled Vehicle," TSME J. of Research and Applications in Mechanical Engineering, Vol.1, No.3, pp. 33-39, 2013.
- "Dynamics and Simulation of RWD Vehicle Drifting at Steady State using BNP-MNC Tire Model," SAE Int. J. of Transportation Safety, Vol.1, No.1, pp. 134-144, 2013.
- "Optimal Control for Steady State Drifting of RWD Vehicle," IFAC Proc. Volumes, Vol.7, pp. 824-830, 2013.

**Membership in Academic Societies:**

- Junior Science Talent Project (JSTP)
  - Society of Automotive Engineers Thailand (TSAE)
- 



**Name:**  
Witaya Wannasuphprasit

**Affiliation:**  
Department of Mechanical Engineering, Chulalongkorn University

**Address:**

254 Phayathai Road, Wangmai, Pathumwan, Bangkok 10330, Thailand

**Brief Biographical History:**

1990 Received Bachelor degree in ME (Honor) from King Mongkut's Institute of Technology Ladkrabang

1993 Received Master degree in ME from Northwestern University

1999 Received Ph.D. in ME from Northwestern University

2000 Post-Doctoral Fellow, Northwestern University

**Main Works:**

- Cobots: Collaborative Robots, Haptic Interface, Intelligent Assisted Devices
- US Patents: 6928336, 6907317, 6813542, 6241462
- Awards: Best Paper Awards: IEEE ICRA 1996, ASME IMECE 1998 (MHED)

**Membership in Academic Societies:**

- Thai Society of Mechanical Engineering (TSME)
  - Society of Automotive Engineers Thailand (TSAE)
-